Scientific report in 2021

Fundamental mechanisms of post-infarction remodeling in old heart at fibroblast population level

The greater longevity achieved by our society has brought the current research to give a particular interest on understanding the fundamental mechanisms underlying ageing, as age is the major risk factor for many pathologies, including cardiovascular disease. Heart disease remains the number one cause of mortality in the Western world, with myocardial infarction (MI)-based injury and subsequent ventricular remodeling and heart failure as the major sequela of this disorder. Despite the importance of fibrosis in CVD, the contribution of cardiac fibroblasts (cFb) to disease progression remains poorly understood and interventions effectively targeting this cell have only recently emerged in the spotlight. Inf-OLD project focuses on the active role of cFb in the ventricular remodeling of old animals and aims to unveil cFb-specific signaling pathways in natural ageing process upon interference with MI and cell therapy.

The main results obtained in the first year are illustrated below:

WP1. Cardiac fibroblasts were isolated from mouse ventricles of young and old animals and comparatively analyzed. The results, summarized in the figures 1 and 2, suggest only minimal aged-related phenotypic changes in culture. Thus, a slight difference was observed in the distribution pattern of αSMA in young- and old-derived cells: while αSMA had a diffuse distribution in young cells, it appeared organized in stress fibers in old counterparts (Figure 1).

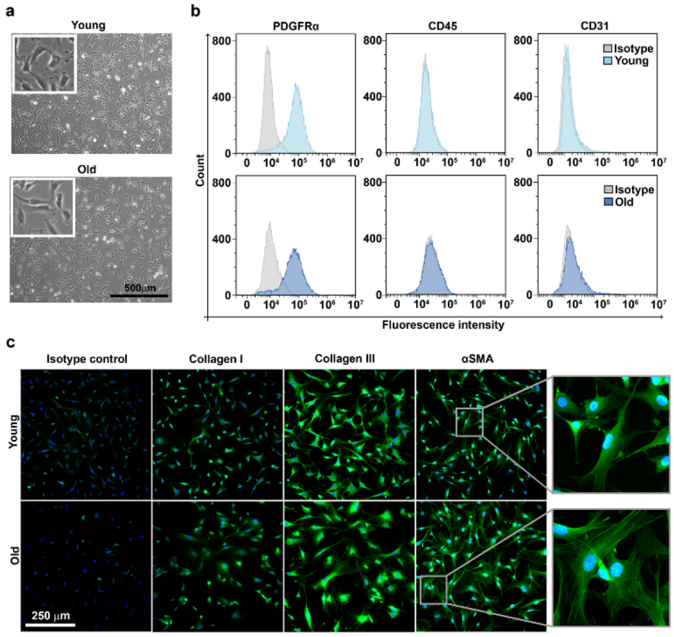

Figure 1. Characterization of cardiac fibroblasts derived from young and old mice. (a) Phase-contrast microscopy of cells after 3 days in culture. No morphological differences were identified between young- and old-derived cells. (b) Flow cytometry analysis of young- and old-derived cells revealing the presence of PDGFRα and the absence of CD31, CD45. (c) Fluorescent microscopy

images illustrating the presence of αSMA, collagen I and collagen III. Note the different patterns of SMA in the two groups (inset).

The evaluation of the cellular metabolism and redox status of old- and young-derived cells showed that no difference existed between young and old cells in terms of ROS production in basal conditions. However, the metabolic analysis using the Seahorse bioanalyzer revealed that old-derived cells had an increased baseline glycolytic activity, in comparison to their young counterparts. Subsequently, in response to mitochondrial stressors, the anaerobic metabolic potential of old cells was reduced (Figure 2).

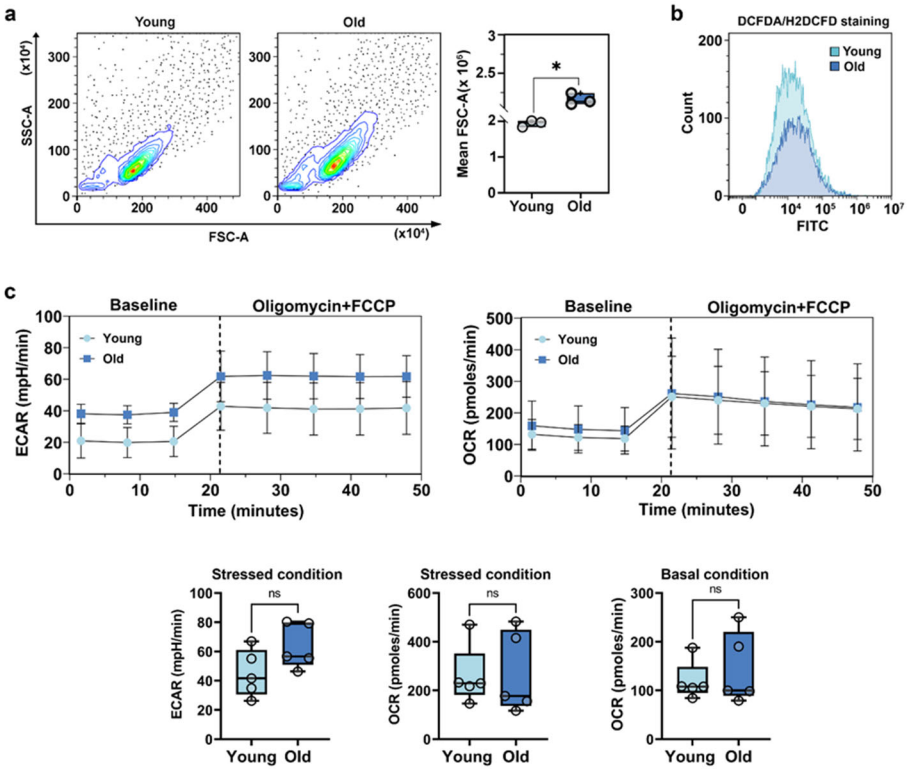

Figure 2. Comparative characterization of mouse cardiac fibroblasts isolated from young and old mice. (a) Scatter plot analysis of cells illustrating the slightly larger size of old-derived cells as compared to young counterparts. (b) Flow-cytometry analysis of ROS production in young- and old-derived cells in basal conditions. (c) Metabolic analysis of cells using the Seahorse bioanalyzer.

WP2. The experimental lot of MI mice (young and old mice with MI and cell transplant) has been obtained and cFb isolated from the cardiac ventricles were used to generate the transcriptome.

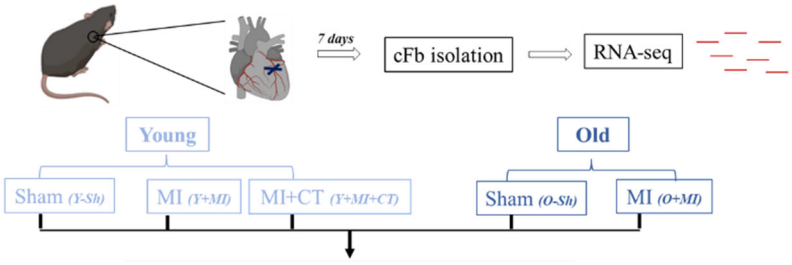

WP3. Aiming at evaluating the cross-talk between cFb and T lymphocytes, in this stage, the protocol for isolation of T cells from splenocytes and the experimental setting for the co-culture between the two populations were standardized. The results are summarized in figures 3 and 4.

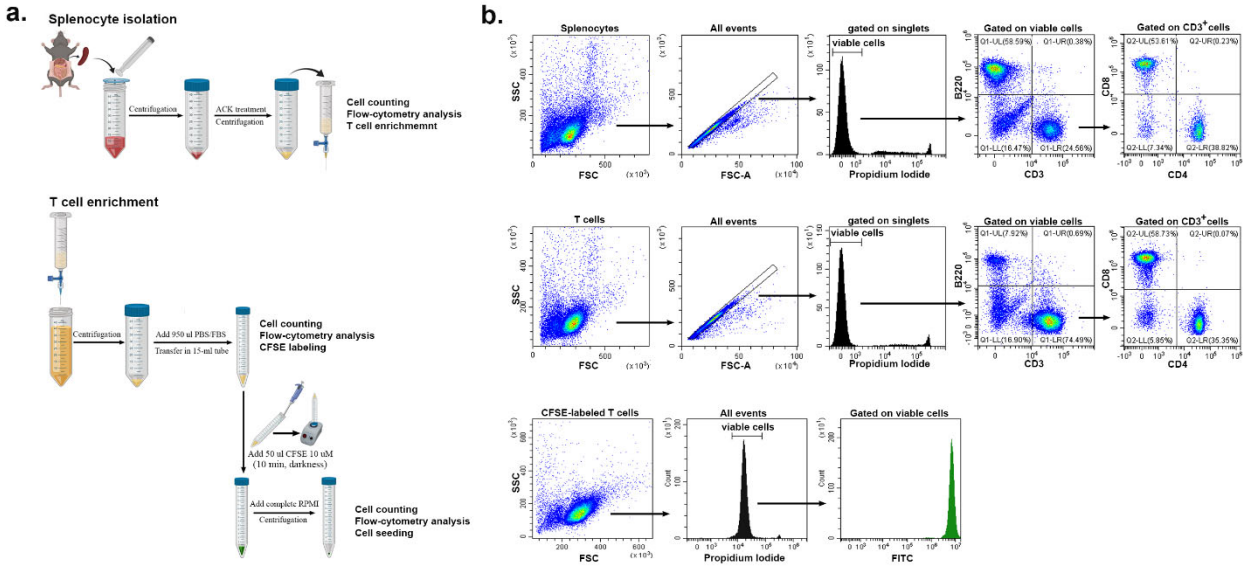

Figure 3. Schematic design of the main steps for T cell isolation and CFSE-labeling. a) Isolation of mouse splenocytes and T cell enrichment on nylon wool column. The critical step of CFSE staining of T cells is also shown. b) Flow-cytometry characterization of splenocytes (upper line), T cells (middle line) and CFSE-labeled T cells (lower line). Note the depletion in B220pos cells in T cell enriched population, as compared to whole splenocyte population (~ 8% B cells after enrichment, as compared to ~ 60% in the initial population) and the relatively unchanged CD8:CD4 ratio after enrichment. Also note the sharp fluorescent peak of T cell population obtained after CFSE staining.

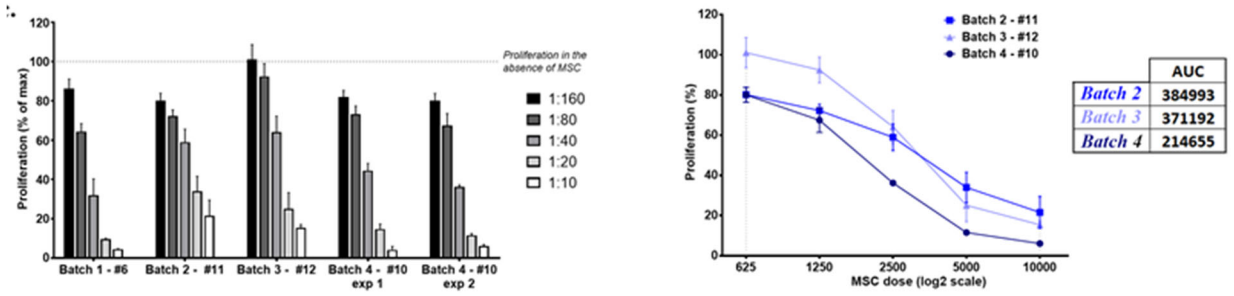

Figure 4. Comparative analysis of the immunosuppressive properties of different batches of MSC. The comparison was done by reporting the proliferation as percentage of maximum proliferation obtained in individual experiments. By plotting the proliferation against the dose of MSC, the area under curve can be calculated, which makes possible the comparison between the immunosuppressive properties of different batches. Lower the AUC, higher the immunosuppressive effects.

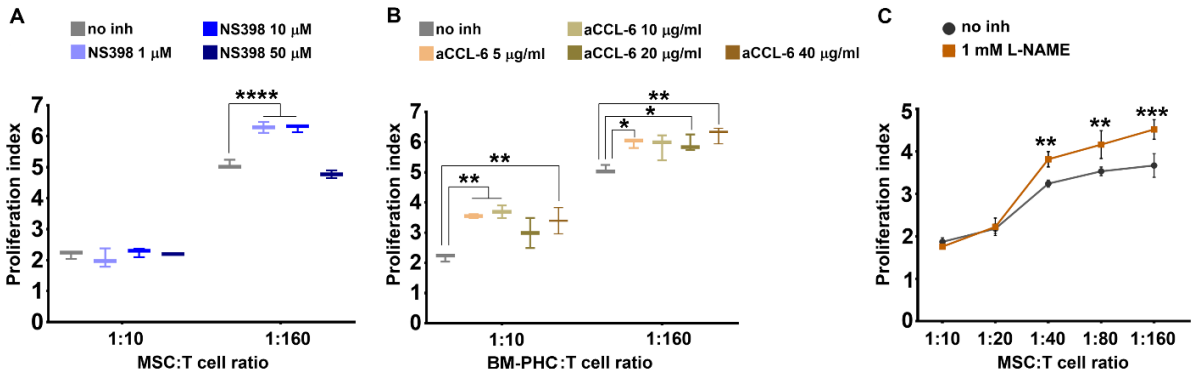

Figure 5. The effects of MSC on T cell proliferation in the presence of inhibitors. *(A) Effect of different doses of NS398, a specific COX-2 inhibitor, on reversing the inhibitory effect of MSC. Note the capacity of NS398 at 1 and 10 μM to partially reverse the MSC effect on T cell proliferation at the lowest MSC: T cell ratio.* ***(B)*** *Effect of different doses of CCL-6 neutralizing antibody on reversing the inhibitory effect of BM-PHC. Note the reversing effects of anti-CCL-6 at both BM-PHC: T cell ratios. The graphics in a-b illustrate a representative experiment from at least four experiments performed with different batches, with the same conclusions.* ***(C)*** *Effect of L-NAME, a specific NO synthase inhibitor, on reversing the inhibitory effect of MSC. The graphic illustrates a representative experiment from three experiments preformed with different L-NAME doses: 100 nM, 500 nM, and 1mM. No dose-dependent effect of L-NAME was observed, yet the three doses produced the same reversing effects.*